

## RESEARCH ARTICLE

# Dielectric and Thermal Response of TiO<sub>2</sub> and SiC Natural Ester Based Nanofluids for Use in Power Transformers

KONSTANTINOS N. KOUTRAS<sup>1</sup>, GEORGIOS D. PEPPAS<sup>2</sup>, (Senior Member, IEEE),  
TIMOTHEOS T. FETSIS<sup>1</sup>, SOKRATIS N. TEGOPOULOS<sup>3</sup>, VASSILIOS P. CHARALAMPAKOS<sup>4</sup>,  
APOSTOLOS KYRITSIS<sup>5</sup>, ANDREAS G. YIOTIS<sup>5</sup>, IOANNIS F. GONOS<sup>6</sup>, (Senior Member, IEEE),  
AND ELEFThERIA C. PYRGIOTI<sup>1</sup>, (Member, IEEE)

<sup>1</sup>High Voltage Laboratory, Department of Electrical and Computer Engineering, University of Patras, 26500 Patras, Greece

<sup>2</sup>Raycap S.A., 66100 Drama, Greece

<sup>3</sup>School of Applied Mathematics and Physical Sciences, National Technical University of Athens, 15780 Athens, Greece

<sup>4</sup>Department of Electrical and Computer Engineering, University of Peloponnese, 26334 Patras, Greece

<sup>5</sup>School of Mineral Resources Engineering, Technical University of Crete, 73100 Chania, Greece

<sup>6</sup>School of Electrical and Computer Engineering, National Technical University of Athens, 15780 Athens, Greece

Corresponding authors: Konstantinos N. Koutras (k.koutras@ece.upatras.gr) and Georgios D. Peppas (peppas@ece.upatras.gr)

**ABSTRACT** The improvement of dielectric and thermal properties of insulating oils used in High Voltage (HV) equipment has been a key part of research over the last three decades. In this study, a natural ester oil is used as matrix oil and dispersions of two semi-conducting nanoparticles (NPs), titanium oxide (TiO<sub>2</sub>) and silicon carbide (SiC), are prepared in 0.004 weight percentage ratio (0.004% w/w). In terms of thermal features, thermal diffusivity and thermal conductivity are measured over a large temperature range between 25 and 90 °C. By means of the dielectric properties, the Lightning Impulse Breakdown Voltage (LI BDV) of nanofluids (NFs) is measured and compared to the corresponding ones of the matrix. Moreover, the dielectric constant and dielectric dissipation factor (DDF) are determined for the NF and matrix samples in the frequency range of 1 to 10<sup>6</sup> Hz. The obtained results show that the NF containing SiC NPs is characterized from the greatest increase in thermal conductivity, by 58% with respect to natural ester oil's, as well as the lowest dielectric constant in both 25 and 90 °C, most likely due to their higher permittivity and thermal conductivity. Lastly, the LI BDV of the same NF is the most enhanced, by 10% relatively to the matrix, while a numerical model in COMSOL Multiphysics is developed and is found to successfully verify the LI BDV results.

**INDEX TERMS** Insulating nanofluid, lightning impulse, dielectric constant, thermal conductivity, numerical model.

## I. INTRODUCTION

Dielectric liquids are one of the three types of insulation used in High Voltage (HV) equipment, due to their high dielectric strength, the greater ease of their replacement in relation to solid insulators and mainly thanks to their ability to dissipate heat preventing the temperature rise inside it [1]. The use of mineral oil as dielectric liquid in HV equipment, mainly power transformers, displays certain disadvantages,

The associate editor coordinating the review of this manuscript and approving it for publication was Santosh Kumar<sup>1</sup>.

such as toxicity, high flammability, while the combination of paper in the conductors leads to anisomeric stress due to the significant deviation in their dielectric constants [2]–[6].

Therefore, current research interests focus on finding a proper replacement, with natural and synthetic esters being possible candidates, as long they are readily biodegradable, they are characterized from increased flash and fire points and their higher permittivity is critical, as it can match the one of paper insulation in minimizing electric stress during high-load conditions [5]–[9]. However, natural ester oils (NEO) suffer from lower dielectric strength under AC or Lightning

Impulse (LI) voltage [9], [10]. Furthermore, as the temperature rises, their dielectric dissipation factor (DDF) rises as well, implying increasing dielectric losses [12], [13]. As a result, researchers are concentrating their efforts on developing nanofluids (NFs) based on conventional oil and a suitable amount of nanoparticles (NPs), with the goal of eliminating ester oil defects while also increasing their dielectric strength and thermal performance [7]–[19].

The integrated NPs are classified on account of their types i.e., metal oxides [7]–[11], [14]–[17], carbides [13], [19], [20] and nitrides [20]–[22], their shapes, sizes and electrical property, i.e. conductive [9]–[11], [15], [23], semi-conductive [8], [13], [14], [17], [24]–[26] and insulative [11], [15], [21], [22], [25]. Khaled and Beroual [11] reported that adding conductive iron oxide (Fe<sub>3</sub>O<sub>4</sub>) NPs with a diameter of 50 nanometers (nm) at 0.2 g/L concentration to synthetic ester oil (SEO) can result in a 7.51% of the negative Lightning Impulse Breakdown Voltage (LI BDV). The same authors [15] observed that integrating the same kinds of NPs in NEO can result in a 48 percent increase of the AC Breakdown Voltage (AC BDV). Koutras *et al.* [13] studied the influence of increasing concentration of silicon carbide (SiC) NPs of 50 nm average diameter in AC BDV of NEO FR3. They found that the AC dielectric strength is increased until a threshold level of 0.004 % w/w and decreased after this concentration level. In [17], Koutras *et al.* found that the addition of titanium oxide (TiO<sub>2</sub>) NPs with 21 nm average diameter in the same NEO can lead to a 22.4% maximum improvement of the AC BDV at 0.020% volume percentage ratio. Primo *et al.* [27] studied the LI BD performance of mineral oil-based Fe<sub>3</sub>O<sub>4</sub> NFs on various concentrations finding that positive LI BDV can be augmented by 50%, but the negative one is similar to the matrix's. Mansour *et al.* [28] studied the influence of surface modified aluminum oxide (Al<sub>2</sub>O<sub>3</sub>) and TiO<sub>2</sub> NPs on AC BDV. They found that with the addition of a suitable amount of surfactant, the same percentage enhancement is recorded, in contrast with the effect of the unmodified NPs, where the integration of TiO<sub>2</sub> led to higher improvement. They also reported similar decrease in dielectric constant for both NFs containing surface-modified NPs, which was attributed to the influence of the augmented interfacial zone. However, the use of surfactants could reduce the heat transfer performance of NFs while simultaneously increasing viscosity [29], [30]. Moreover, Khelifa *et al.* [18] and Atiya *et al.* [31] studied Partial Discharge (PD) activity in SEO and mineral oil-based NFs respectively. The authors of [18] found that the addition of fullerene NPs significantly enhances the Partial Discharge Inception Voltage (PDIV) of SEO, unlike graphene NPs, while the authors of [31] reported that Al<sub>2</sub>O<sub>3</sub> NPs could cause a higher improvement to the resistance of NF to PD activity with respect to TiO<sub>2</sub>. They attributed this finding to the larger Electrical Double Layer (EDL) thickness around the Al<sub>2</sub>O<sub>3</sub> NPs [31]. Beyond liquid insulation, NPs are also widely used to increase the dielectric properties of solid insulators [32]–[34] and in other types, like biosensors [35]–[37].

In this work, two uniform suspensions of SiC and TiO<sub>2</sub> NPs at 0.004% w/w are prepared in NEO FR3. In terms of thermal properties, thermal diffusivity and thermal conductivity are measured and calculated respectively. In terms of the dielectric ones, the relative permittivity and electrical conductivity of the NPs and matrix are measured by employing the Dielectric Relaxation Spectroscopy (DRS) technique. LI BDV under positive polarity, pursuant to IEC 60897 standard is also examined and compared to the matrix performance. Apart from that, the dielectric constant and DDF are determined with the DRS technique. The novelty of this study can be supported from the following points:

- In the literature, the BDV characteristic and mechanism of natural ester-based NFs incorporating metal oxide NPs, particularly TiO<sub>2</sub>, have been extensively studied [26], [38]. The impact of carbide NPs, such as SiC, a semiconductor NP like TiO<sub>2</sub>, in biodegradable oils, on the other hand, has not been thoroughly investigated [13].
- Most research studies are focused on the dielectric properties of NFs, while the available literature of their effect on thermal diffusivity is limited [21], [22], [39], [40]. Consequently, investigating the dielectric and thermal performance of semiconducting SiC NP doped NF, compared to the corresponding one of NF incorporating TiO<sub>2</sub> NPs in the same concentration leads to valuable findings.
- One of the most significant drawbacks of the NEO is its high dielectric losses. With the assistance of the DRS method, it has been shown that the DDF of both NFs, especially sNF, is reduced mainly at 25 °C.
- Last but not least, the conduction of the LI BDV experiment under positive polarity is accompanied with the development of a numerical model for the simulation of pre-breakdown phenomena regarding the same NFs during LI stress in COMSOL Multiphysics [23], [41] and the results are compared to the experimental ones. The reported results demonstrate that adding SiC NPs to the under-studied oil can result into an improvement of the dielectric properties, while the development of the model in COMSOL Multiphysics provides physical insight on the pre-breakdown phenomena and verifies the LI BDV results.

## II. CHARACTERIZATION OF THE MATERIALS AND SYNTHESIS OF NANOFUIDS

Biodegradable NEO FR3<sup>TM</sup> has been used as matrix, with a density of 0.92 g/ml, fire point greater than 300 °C and other characteristics that have been discussed elsewhere [10], [17], [42]. The commercially obtained TiO<sub>2</sub> (Sigma Aldrich) and SiC (NanoAmor) NPs are spherical, with 99.5% purity and average nominal diameters of 21 and 50 nm respectively. The thermal conductivity of the integrated TiO<sub>2</sub> and SiC NPs is in the range of 5–11.8 W/(m·K) and 165–220 W/(m·K) respectively. The Field Emission Scanning Electron Microscopy

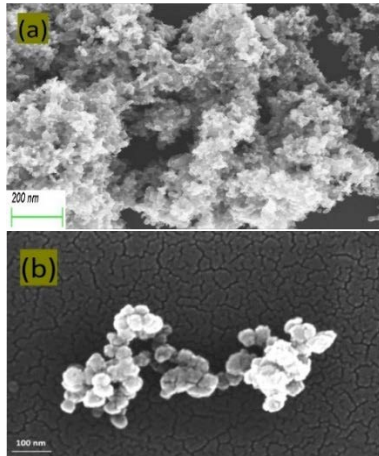


FIGURE 1. FE-SEM images of the NPs in high magnifications: (a) TiO<sub>2</sub> NPs, (b) SiC NPs.

(FE-SEM) method was used to determine the nominal size of the NPs. The NPs were drop-casted onto Si substrates and a Zeiss SUPRA 35VP microscope was utilized to monitor their size. Figure 1 depicts the TiO<sub>2</sub> and SiC powders as shown by FE-SEM, revealing that their average size is in the range of the nominal one.

**A. PREPARATION PROCEDURE OF NANOFUIDS**

For the production of NF samples, a two-step procedure is employed. A 500 mL volume of FR3 has been chosen as the matrix for the production of colloidal suspensions. To accomplish moisture reduction within the allowed limits, each sample is filtered and dried overnight in a hot air oven at 120 °C. Following the methods described previously [10], the amount of moisture inside each sample after drying was validated using the Karl Fischer titration method [43]. In summary, the residual moisture was measured and validated using a Mitsubishi Chemicals Co. CA-100 moisture meter and a Metrohm KF Coulometer 831, respectively and was found less than 200 ppm.

Following that, suitable proportions of TiO<sub>2</sub> and SiC powder are submerged in the matrix dielectric liquid to attain the selected 0.004% w/w concentration. However, the integrated colloids tend to aggregate rapidly after their addition because of the attractive intermolecular forces, creating agglomerates, due to their large surface areas per unit volume [10]–[13], [26]. Consequently, the NF samples are ultrasonicated for 1.5 h using Elma’s ultrasonic cleaner Elmasonic S 40 H in order to guarantee initial homogeneous colloidal suspension dispersion. Table 1 displays the labeling of the NFs, as well as a base oil sample that is also investigated for comparison purposes.

**B. ELECTRICAL CHARACTERIZATION OF MATERIALS**

The DRS method is used to measure the real and imaginary parts of relative permittivity for the NPs and matrix sample. The NPs in form of powder are placed in a special cell with

TABLE 1. Labeling of under-study samples.

Sample Label (n)	NPs Percentage Ratio (% w/w)
Matrix (Base)	0
tNF	NF containing 0.004% TiO <sub>2</sub>
sNF	NF containing 0.004% SiC

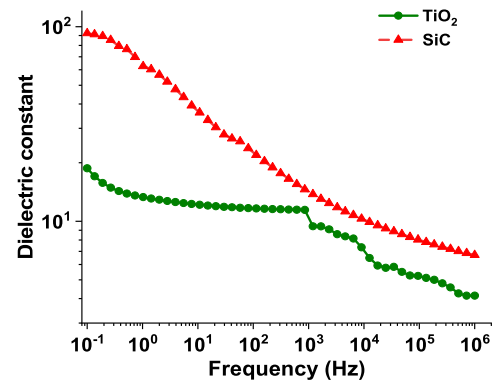


FIGURE 2. Change of dielectric constant versus frequency for: (a) the used NPs, (b) the matrix.

golden sphere electrodes of 20 mm diameter, which is then inserted to the Novocontrol BDS1200 cell for the conduction of the measurements. The liquid samples, on the other hand, are put in a sample holder-capacitor that is cylindrical (BDS1307 cylindrical liquid cell by Novocontrol). Using a Novocontrol Alpha analyzer, an AC voltage is applied to the capacitor sample, and the relative permittivity  $\epsilon_r$ , in the form of (1), is recorded as a function of frequency in the range from 1 to 10<sup>6</sup> Hz [44]:

$$\epsilon_r = \epsilon_r' - j\epsilon_r'' \tag{1}$$

where,  $\epsilon_r'$  represents the real part of relative permittivity expressing the dielectric constant and  $\epsilon_r''$  denotes the imaginary part, which defines the dielectric losses caused by leakage current and dielectric polarization. In addition, the DDF ( $\tan\delta$ ), is calculated from (2):

$$\tan\delta = \frac{\epsilon_r''}{\epsilon_r'} \tag{2}$$

The electrical conductivity  $\sigma$  in S·m<sup>-1</sup>, on the other hand, is calculated from the measured dielectric losses, according to (3):

$$\sigma = \omega \cdot \epsilon_0 \cdot \epsilon_r'' \tag{3}$$

where,  $\omega$  is the angular frequency in rad/s and  $\epsilon_0$  is the permittivity of vacuum in F·m<sup>-1</sup>.

Figures 2 and 3 illustrate the dielectric constant and electrical conductivity of the NPs at room temperature, respectively.

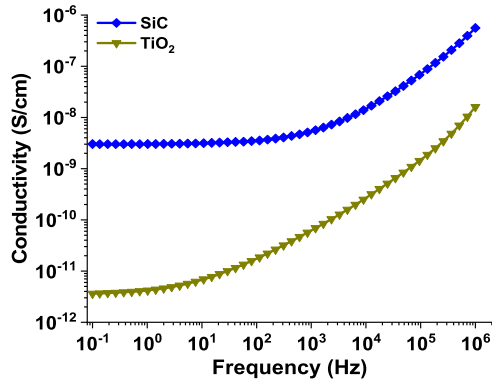


**FIGURE 3.** Change of electrical conductivity versus frequency for: (a) the used NPs, (b) the matrix.

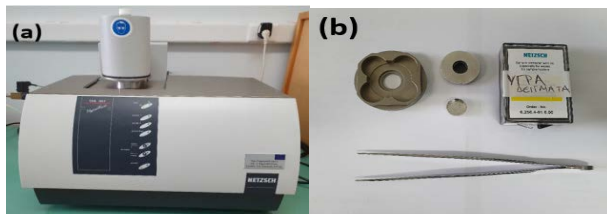


**FIGURE 4.** (a) NETZSCH LFA 467 Hyper Flash apparatus, (b) LFA test cell along with the liquid samples.

### III. EXPERIMENTAL SETUP

Firstly, both the thermal and dielectric measurements were conducted inside the first 48 hours from the synthesis of uniform suspensions, in order to eliminate the negative effects of NPs' ageing which leads to aggregation/sedimentation, thus change in the active NPs' concentration inside the transformer oil [13], [17], [45].

The thermal diffusivity and thermal conductivity are determined using a NETZSCH LFA 467 Hyper Flash apparatus, as depicted in Figure 4(a). The samples are placed in a liquid-specific cell (LFA test cell with diameter of 12.7 mm) illustrated in Figure 4(b). Measurements are performed across a wide range (from 25 to 85 °C in 10-degree increments, with a final temperature of 90 °C). Thermal diffusivity  $\alpha$ , in mm<sup>2</sup>/s, is directly measured from an average of 5 light pulse shots and calculated via the half-time method (4) [45]:

$$\alpha = \frac{1.38 \cdot L^2}{\pi^2 \cdot t_{1/2}} \quad (4)$$

where,  $L$  is the sample thickness and  $t_{1/2}$  is the half-time necessary in order the maximum temperature to reach on the opposite side.

Thermal conductivity  $\lambda$ , on the other hand, is calculated from Fourier's law of heat conduction (5) [42], [45]:

$$\lambda = \alpha \cdot C_p \cdot \rho \quad (5)$$

where,  $\lambda$  is the thermal conductivity in W/(m·K),  $C_p$  is the specific heat capacity in J/(g·K) and  $\rho$  is the density of the liquid in g/ml, which has been kept constant and equal to that of the matrix (i.e. 0.92 g/ml).

The dielectric constant and DDF of the NF samples have been determined in the same way as described in the previous section for the NPs and matrix oil with the DRS technique. The NF samples are placed in a cylindrical liquid sample holder-capacitor. An AC voltage is applied to the capacitor sample and the relative permittivity  $\epsilon_r$  is recorded as a function of frequency, in the range from 1 Hz to 1 MHz employing a Novocontrol Alpha analyzer.

In terms of LI BDV measurement, this is a critical attribute because it indicates the dielectric insulation coordination of the NF during lightning activity. A two-stage (Marx) Hae-fely LTD impulse generator with a 400 kV maximum output voltage, 15 nF per stage capacitance and 600 J total energy, is used [46]. The measurements are conducted with a divergent field geometry, under positive polarity, according to the IEC 60897 standard [47]. The test cell consists of point-sphere electrodes and their gap is fixed at 25 mm. The point's radius of curvature is 50  $\mu$ m and the diameter of the sphere is 12.7 mm.

For the conduction of the experiment, the up and down method is implemented [11], [27], [48]. Starting from a relatively low voltage with respect to the expected LI BDV, 3 voltage applications take place at each voltage level. In case none of the 3 ends in breakdown, the voltage increases by 5 kV. If at least 1 BD occurs, then the voltage is automatically reduced by 2 kV and a 5 min interval is applied before the next shot. The same process continues until 10 BD events are obtained, followed by statistical analysis with their adjustment to the Weibull distribution [11], [15], [17], [27], [48]. The equivalent circuit of the impulse generator is shown in Figure 5(a). The applied LIV (1.2/50  $\mu$ s) is monitored via the CST capacitive divider (Figure 5(a)) through an oscilloscope Tektronix DPO4104; 1 GHz/5 GS s-1. A typical positive LI BDV waveform obtained from the oscilloscope is presented in Figure 5(b).

For the processing of the results, the Weibull distribution was chosen in order to evaluate the strength of the matrix oil and NF samples in critical failure rates of 1, 10, and 50% since it does not make assertions on skewness and kurtosis [11], [13], [15]. In order for this statistical processing to be feasible, the Anderson-Darling goodness of fit test is used to conclude whether the BD data for each sample can be adjusted to the Weibull distribution by calculating the  $p$ -value [13] and comparing it to the selected significant level  $\alpha$ , which is determined to be 5% ( $\alpha = 0.05$ ).

## IV. EXPERIMENTAL RESULTS AND DISCUSSION

### A. THERMAL PROPERTIES

This section includes the obtained results from the thermal diffusivity and conductivity measurements, along with the thermal stability study and discussion on them.

#### 1) THERMAL DIFFUSIVITY AND CONDUCTIVITY

The mean values of thermal diffusivity for the NF and base oil samples acquired from five light pulses and calculated

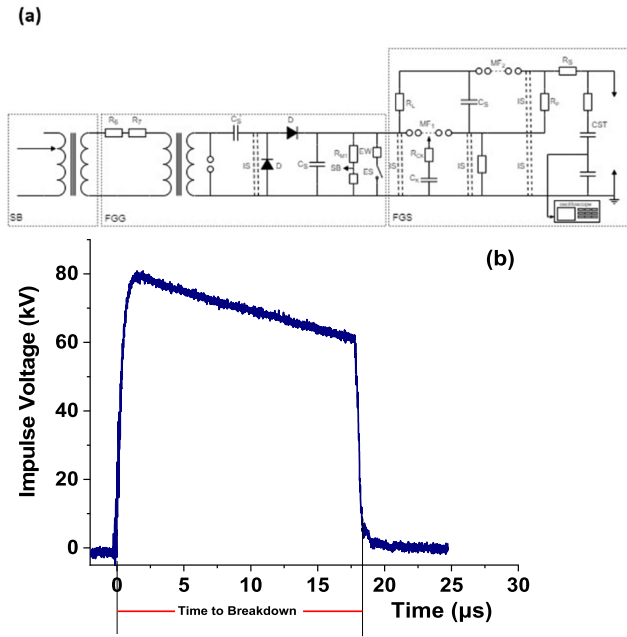


FIGURE 5. (a) Equivalent circuit of the impulse generator, (b) Typical LI waveform (1.2/50 μs) displaying the breakdown time.

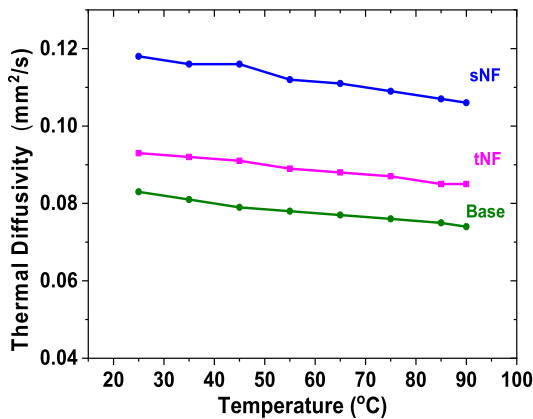


FIGURE 6. Change of the thermal diffusivity of the samples in question as a function of temperature (range 25-90 °C).

from (4) at each temperature level are demonstrated in Figure 6. It is clear from this graph that both NF samples have improved thermal diffusivity with respect to NEO, with sNF showing the higher improvement throughout the whole temperature range. Beyond that, as the temperature rises, all samples show a decrease in diffusivity [45], [49], [50]. The Matrix oil sample has the greatest impact on the thermal diffusivity behavior of NFs, as evidenced by the experimental results, as long the same trend in thermal diffusivity with temperature increase is also observed for the NFs [50].

Figure 7 shows the thermal conductivity of the samples under investigation as a function of temperature. It appears that for both NF and matrix oil samples, it remains nearly constant (with very slight variances) over the whole temperature range. The highest thermal conductivity augmentation is

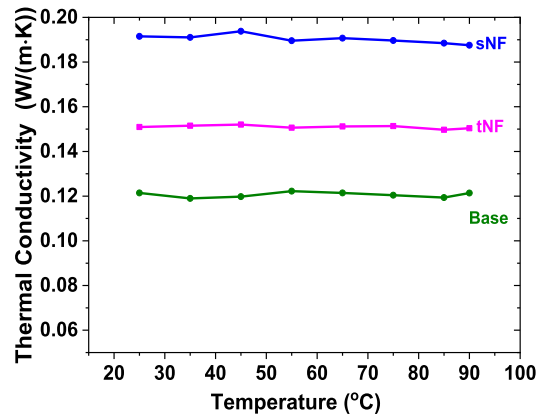


FIGURE 7. Change of the thermal conductivity of the samples in question as a function of temperature (range 25-90 °C).

seen in the sNF sample, which is around 58% with respect to the NEO's, while the corresponding increase regarding tNF is about 25%. Therefore, it is obvious that at this weight percentage, the integration of this type of NPs has led to significant thermal conductivity enhancement of the dielectric liquid. This finding is consistent with several published research works regarding the influence of nanometric scale particles in thermal conductivity [20], [21], [39], [40], [50]. The high thermal conductivity of the SiC NPs (165-220 W/(m· K)) with respect to TiO<sub>2</sub> could be responsible for the higher improvement concerning the sNF sample [51], [52]. Thermal behavior of the two NF samples at these concentration levels is directly affected from the NPs, since they do not suffer from rapid aggregation, as it has been shown in our previous works [13], [17], [50], [53]. When NPs cluster, they lose their ability to increase heat transmission, alter the structural distribution of the suspension system, and ultimately break the irregular movement laws [52].

### B. DIELECTRIC PROPERTIES

This part includes the obtained results from the permittivity and DDF measurements, as well as the analysis of positive LI BDV and PD activity results.

#### 1) DIELECTRIC CONSTANT AND DISSIPATION FACTOR

Figures 8(a)-(b) show the spectral change in the real part of relative permittivity for the under-studied samples at 25 and 90 °C, respectively. The corresponding change of DDF versus frequency at the same temperatures is depicted in Figures 10(a)-(b) respectively.

From Figures 8(a)-(b) it is apparent that both NF samples, especially sNF, are characterized from lower dielectric constant for the whole frequency range, including the power frequency of 50 (60) Hz, mainly attributed to interfacial polarization of Maxwell-Wagner-Sillars type and to electrode polarization [42]. The decreased values of dielectric constant could be a sign for improved dielectric strength of this sample [13], [28], which is also reflected in the following LI

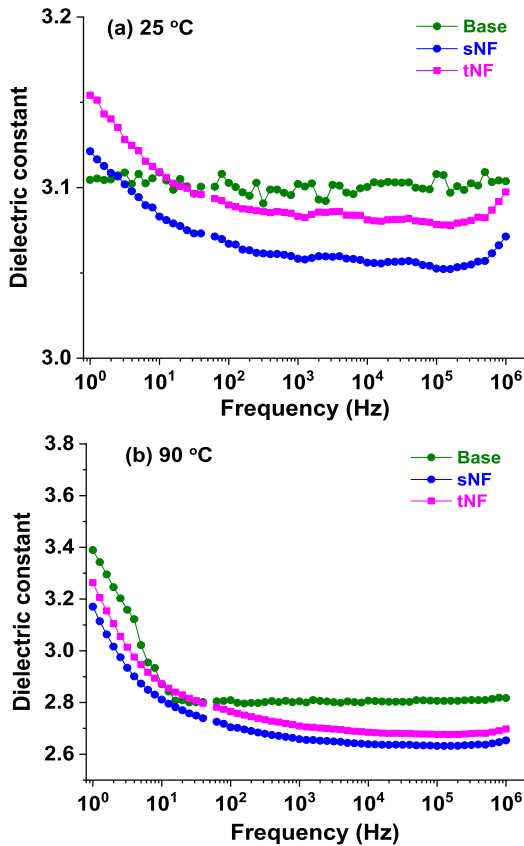


FIGURE 8. Spectral change of dielectric constant of the samples in question (range 1-10<sup>6</sup> Hz): (a) at 25 °C, (b) at 90 °C.

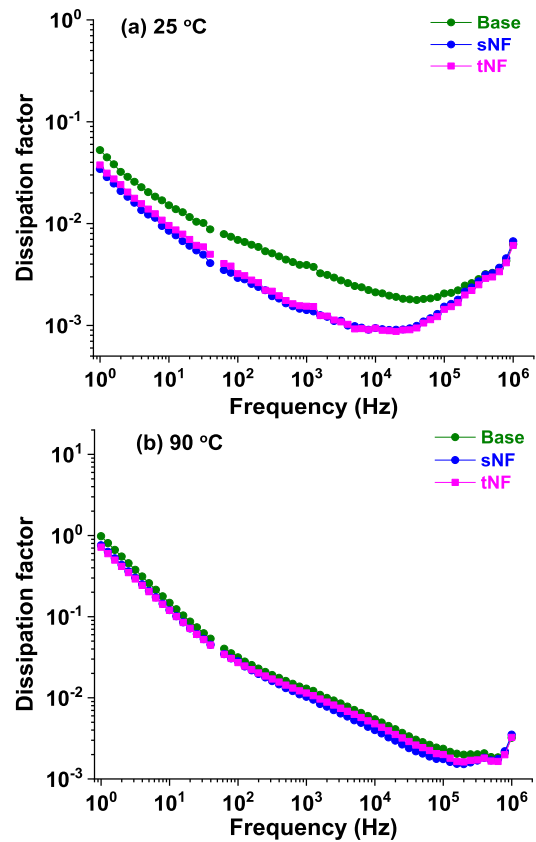


FIGURE 9. Spectral change of dissipation factor of the samples in question (range 1-10<sup>6</sup> Hz): (a) at 25 °C, (b) at 90 °C.

BDV results. It is also obvious that the dielectric constant falls with increasing temperature in all under-study samples, therefore they are more insulative with temperature rise. The temperature effect could be attributed to the fact that, dipolar orientation polarization processes taking place in this frequency range, are proportional to 1/T [50]. Assuming that this type of polarization is the main contributor to polarizability, the recorded dielectric constant reduction with temperature increase can be explained.

Figures 9(a)-(b) show that both NF samples exhibit lower DDF over the whole frequency range, with a greater reduction at room temperature. This is a key characteristic because the elevated DDF in relation to mineral oil is one of the NEO’s most serious shortcomings [12], [13]. It should be emphasized, however, that all samples show an increase in DDF as the temperature rises. The DDF, directly correlated with the electrical conductivity of both NFs is mainly driven from the matrix dielectric liquid electrophoresis conductivity [50].

2) LIGHTNING IMPULSE BREAKDOWN VOLTAGE

Table 2 presents the mean values of LI BDV in kV and time to breakdown in  $\mu s$ , regarding the samples in question. In the same Table, the standard deviation of them, is also demonstrated. Scale and shape parameters are crucial for

TABLE 2. Descriptive statistics of the lightning impulse breakdown experiment.

Sample type	LI BDV (kV)		Breakdown Time ( $\mu s$ )		Breakdown velocity (km/s)		
	Mean (kV)	Std. Dev. (kV)	Mean ( $\mu s$ )	Std. Dev. ( $\mu s$ )	U <sub>50%</sub>	U <sub>10%</sub>	U <sub>1%</sub>
Matrix oil	75.3	2.6	17.5	1.3	1.47	1.64	1.91
tNF	79.5	2.0	18.4	1.0	1.35	1.48	1.65
sNF	82.7	2.4	19.1	1.1	1.30	1.43	1.63

the Weibull distribution and represent the failure at a rate of 63.2% and the dispersion of the events (Weibull slope), respectively [11], [13], [15]. The breakdown velocities at 50, 10 and 1% probability levels after fitting the breakdown times to the Weibull distribution are also presented in Table 2. Table 3 also contains the corresponding values of p-value, where it seems that all of them are higher than the significant level, meaning that the possibility that the BD events follow the Weibull distribution cannot be rejected, as well as the values of scale and shape parameters.

Consequently, from the Weibull plot of the LI BDV of Matrix oil, tNF and sNF samples (Figure 10), the BDV at failure probabilities of 1, 10 and 50% are calculated and included in Table 4. According to the processing of the LI BDV results, it is evident that the mean LI BDV is augmented with the addition of SiC NPs at 0.004% w/w with respect

TABLE 3. Weibull distribution parameters.

Sample Label (n)	p-value	Scale (kV)	Shape
Matrix oil	0.07	76.6	28.9
tNF	0.25	80.4	48.0
sNF	0.18	83.9	33.0

TABLE 4. Withstand voltages based on the weibull distribution.

Sample Label (n)	U <sub>50%</sub> (kV)	U <sub>10%</sub> (kV)	U <sub>1%</sub> (kV)
Matrix oil	75.6	70.8	65.3
tNF	79.8	76.8	73.1
sNF	83.0	78.3	73.0

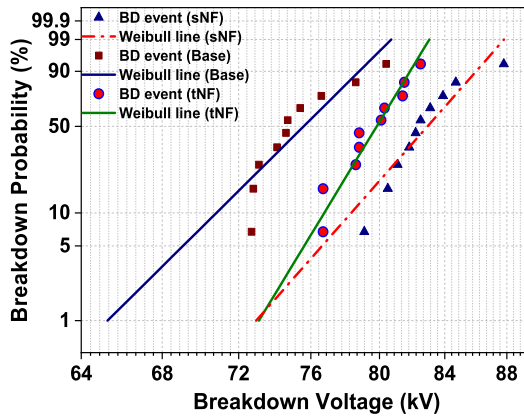


FIGURE 10. Weibull plot of the LI breakdown events for the matrix and the two nanofluid samples under investigation.

to NEO's by 9.8%, while the addition of TiO<sub>2</sub> NPs at the same weight percentage ratio leads to lower improvement, by 5.6%. Furthermore, on account of the withstand voltages calculated following adjustment of the BD events to the corresponding Weibull distribution, it has been found that U<sub>10%</sub> and U<sub>1%</sub> of sNF the highest improvement, by 10.6% and 11.8% with respect to the matrix oil. The importance of these values is critical for the insulation coordination and the design of a high voltage insulation system with operational reliability and reproducibility of the dielectric insulator's performance. Particularly the U<sub>10%</sub> and U<sub>1%</sub>, corresponding to the lower BDV level, guarantee the insulation level of the system [54], [55].

BDV at 10% cumulative probability provides an assessment for the lowest possible BDV, therefore it is an indication for the transition of streamer to the 2<sup>nd</sup> mode [10], [11], [13], [15], [18], [24], [56], while U<sub>1%</sub> refers to the transformer's voltage limit for safety and continuing functionality, which is a vital parameter for power system insulation coordination during lightning and surge incidents [57], [58].

The average breakdown velocity  $u$  in  $m \cdot s^{-1}$ , across the gap of 2.5 cm can be calculated from (6) [27], [59], [60]:

$$\bar{u} = \frac{d}{t} \tag{6}$$

where,  $d$  is the gap length in m, i.e. 2.5 cm, and  $t$  is the mean time to BD in s, as it is demonstrated for each sample in Table 2. The average breakdown velocity for Matrix oil, tNF and sNF is calculated as 1.47, 1.36 and 1.31  $km \cdot s^{-1}$  respectively corresponding to slow streamers propagation (2<sup>nd</sup> mode) [59], [60].

In order to interpret the obtained LI BDV results, the NP mechanism as shallow traps of the charge carriers, will be employed [23], [25]. Under the application of an external electric field  $E_0$  in  $V \cdot m^{-1}$ , if the dielectric constant of the integrated NPs and the matrix differs significantly, based on (7), induced or polarized charges are created at the NPs' interface. As long both kinds of NPs are semi-conductive, the existence of surface charges is due to dielectric polarization [25]. These charges produce a potential well, which decreases with the distance from the NP's radius. Therefore, the fast electrons at the streamer's tip are captured in shallow traps and the streamer propagation is slowed down; as a result, a greater electric field value should be provided to allow the electrons to be freed and span the gap. The potential well distribution for both kinds of NPs is expressed from (7), while (8) corresponds to the charge captured by each of them as a function of time [23], [25], [53]:

$$\varphi(r) = \frac{\epsilon'_2 - \epsilon'_1}{2\epsilon'_1 + \epsilon'_2} R^3 E_0 \frac{1}{r^2} \tag{7}$$

where,  $\epsilon'_1$ ,  $\epsilon'_2$  are the dielectric constants of matrix oil and NPs, respectively,  $R$  is the radius of the NP in nm and  $r$  is the distance from the NP's surface in nm.

$$Q(t) = Q_s \frac{\frac{t}{\tau_{pc}}}{1 + \frac{t}{\tau_{pc}}} \tag{8}$$

where,  $Q_s$  is the saturation charge captured by each SiC or TiO<sub>2</sub> NP, expressed by (9), and  $\tau_{pc}$  is the time constant of NP charging, given by (10) [23], [25]:

$$Q_s = -12\pi \epsilon'_1 E_0 R^2 \frac{\epsilon'_2}{2\epsilon'_1 + \epsilon'_2} \tag{9}$$

$$\tau_{pc} = \frac{4\epsilon'_1}{|\rho_e| \mu_e} \tag{10}$$

where,  $\rho_e$  is the electron charge density in  $C \cdot m^{-3}$  and  $\mu_e$  is the electron mobility in  $m^2 \cdot V^{-1} \cdot s^{-1}$ .

Thus, based on Eq. (7) and (9), as long the measured value of dielectric constant of SiC is higher than the one of TiO<sub>2</sub> for the whole frequency range, pursuant to the results of DRS technique (Figure 2(a)), a higher potential well distribution, i.e. a higher local field, is created, especially close to their surface, where more electrons are captured and reduce their mobility, so the streamer propagation is hindered. In order to investigate the latter, a model of a single spherical NP is examined in COMSOL Multiphysics graphic environment. A DC external field has been applied to the y-axis and the electric field distribution has been recorded graphically (Figure 11) and in 3D (Figure 12(a)-(b)). It is apparent that higher electric field values are recorded at the surface of SiC NPs, as expected.

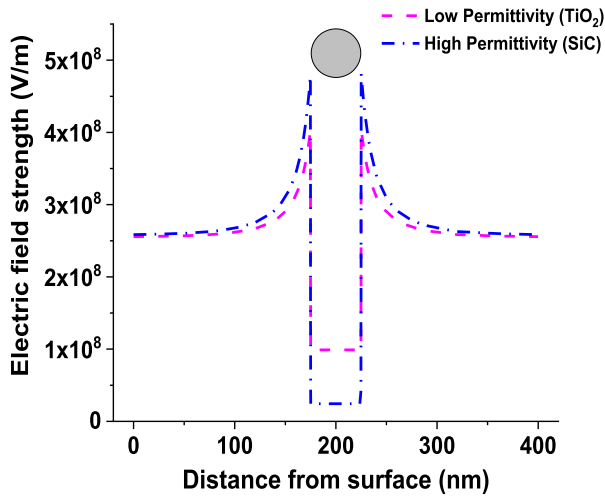


FIGURE 11. Simulated electric field distribution around the surface of SiC and TiO<sub>2</sub> NP.

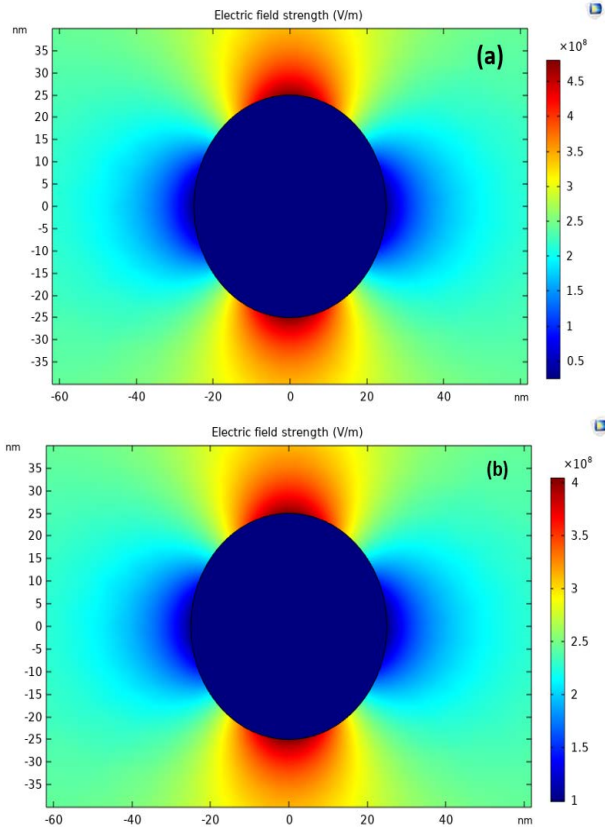


FIGURE 12. 3D plot of electric field distribution around each NP: (a) TiO<sub>2</sub> NP, (b) SiC NP.

V. NUMERICAL MODEL

For the conduction of the simulations, the measured values of dielectric constants from the DRS method have been used for the transformer oil, SiC and TiO<sub>2</sub> NPs for the first return stroke at 25 kHz, based on IEC 62305-4 standard, i.e. 3.1, 9.2 and 5.8 respectively [61]. A point-sphere model in conso-

TABLE 5. Main simulation parameters.

Symbol	Quantity	Value (S.I.)
$\mu_+$	positive ion mobility	$10^{-9} \text{ m}^2 \cdot \text{V}^{-1} \cdot \text{s}^{-1}$
$\mu_-$	negative ion mobility	$10^{-9} \text{ m}^2 \cdot \text{V}^{-1} \cdot \text{s}^{-1}$
$\mu_e$	electron mobility	$10^{-4} \text{ m}^2 \cdot \text{V}^{-1} \cdot \text{s}^{-1}$
$\mu_{np}$	nanoparticle mobility	$10^{-9} \text{ m}^2 \cdot \text{V}^{-1} \cdot \text{s}^{-1}$
$R_{pp}$	ion-ion recombination rate	$1.13 \times 10^{-17} \text{ m}^3 \cdot \text{s}^{-1}$
$R_{pe}$	ion-electron recombination rate	$5.65 \times 10^{-13} \text{ m}^3 \cdot \text{s}^{-1}$
$\alpha$	molecular separation distance	$3 \times 10^{-10} \text{ m}$
$h$	Planck's constant	$6.626 \times 10^{-34} \text{ m}^2 \cdot \text{kg} \cdot \text{s}^{-1}$
$m^*$	effective electron mass	$9.11 \times 10^{-32} \text{ kg}$
$n_0$	number density of ionizable species	$10^{21} \text{ m}^{-3}$
$\Delta/e$	ionization potential	7.1 eV
$\tau_a$	electron- oil molecule attachment time constant	$2 \times 10^{-7} \text{ s}$
$\tau_{np}$	nanoparticle attachment time constant	$2 \times 10^{-9} \text{ s}$

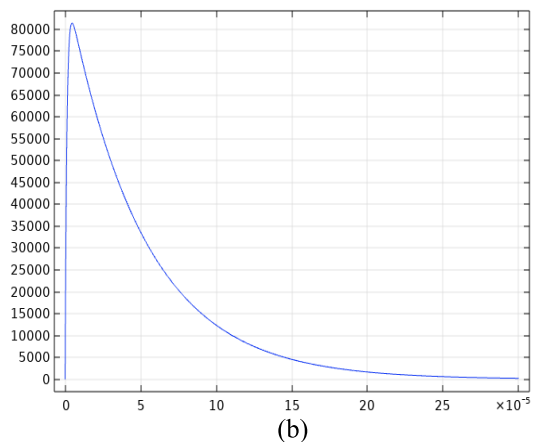
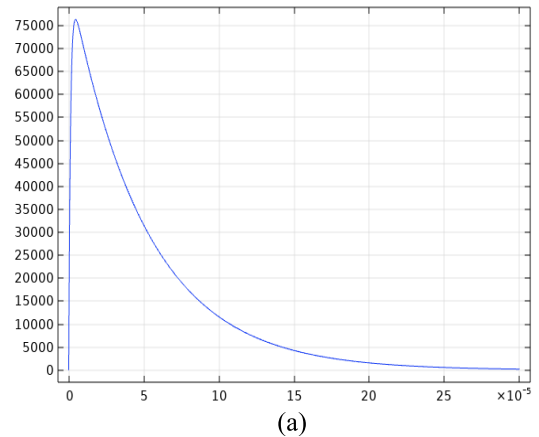
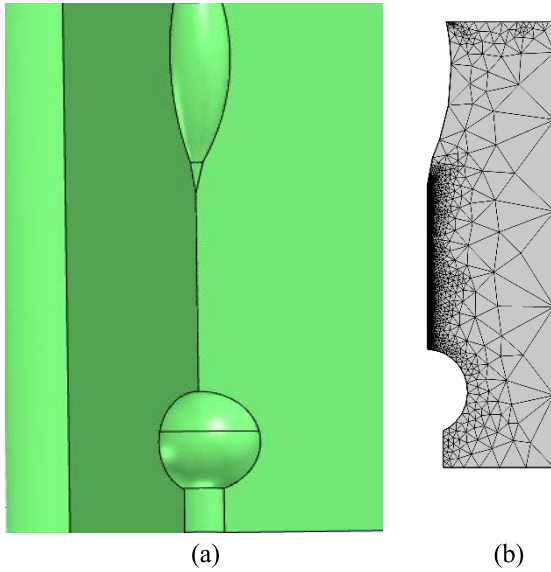


FIGURE 13. Lightning Impulse waveforms for the two simulation cases: (a) 75 kV, 1.2/50  $\mu\text{s}$ , (b) 80 kV, 1.2/50  $\mu\text{s}$ .

nance with the IEC 60897 standard was inserted in COMSOL Multiphysics software and the interfaces *Electrostatics* and *Transport of Diluted species* were used. The charge continuity equations for positive ions (12), negative ions (13), electrons (14) and charged NPs (15) that are related to Gauss'



**FIGURE 14.** (a) Point-sphere gap in COSMOL Multiphysics environment before the application of Lightning Impulse Voltage, (b) Mesh distribution across the gap.

law (11) were introduced to model the LI behavior of pure oil and the corresponding NFs [23], [25], [41], [62], [63]:

$$\begin{aligned} \nabla \cdot (\epsilon_1' \cdot \vec{E}) &= \rho_+ + \rho_- + \rho_e + \rho_{np} \end{aligned} \quad (11)$$

$$\begin{aligned} \frac{\partial \rho_+}{\partial t} + \nabla \cdot (\rho_+ \cdot \mu_+ \cdot \vec{E}) &= G_I(|\vec{E}|) + \frac{\rho_+ \cdot \rho_e \cdot R_{pe}}{e} + \frac{\rho_+ \cdot \rho_- \cdot R_{pn}}{e} \end{aligned} \quad (12)$$

$$\begin{aligned} \frac{\partial \rho_-}{\partial t} - \nabla \cdot (\rho_- \cdot \mu_- \cdot \vec{E}) &= \frac{\rho_e}{\tau_\alpha} - \frac{\rho_+ \cdot \rho_- \cdot R_{pn}}{e} \end{aligned} \quad (13)$$

$$\begin{aligned} \frac{\partial \rho_e}{\partial t} - \nabla \cdot (\rho_e \cdot \mu_e \cdot \vec{E}) &= -G_I(|\vec{E}|) - \frac{\rho_+ \cdot \rho_e \cdot R_{pe}}{e} \\ &\quad - \frac{\rho_e}{\tau_\alpha} - \frac{\rho_e}{\tau_{np}} [1 - H(p_{np,sat} - p_{np})] \end{aligned} \quad (14)$$

$$\begin{aligned} \frac{\partial \rho_{np}}{\partial t} - \nabla \cdot (\rho_{np} \cdot \mu_{np} \cdot \vec{E}) &= \frac{\rho_e}{\tau_{np}} [1 - H(p_{np,sat} - p_{np})] \\ &\quad - \frac{\rho_+ \cdot \rho_{np} \cdot R_{pn}}{e} \end{aligned} \quad (15)$$

where,  $\rho_+$ ,  $\rho_-$ ,  $\rho_e$  and  $\rho_{np}$  stand for positive ion, negative ion, electron, and charged NP densities, respectively. The charging process of the NPs is characterized by the Heaviside function  $H(\rho_{np,sat} - \rho_{np})$  (16), and the saturation charge density  $\rho_{np,sat} = n_{np} \cdot Q_s$ , where  $n_{np}$  is the NPs' number density and  $Q_s$  is expressed from (9). The TiO<sub>2</sub> and SiC NPs' charging density limit was calculated as -277 and -359 C/m<sup>3</sup> respec-

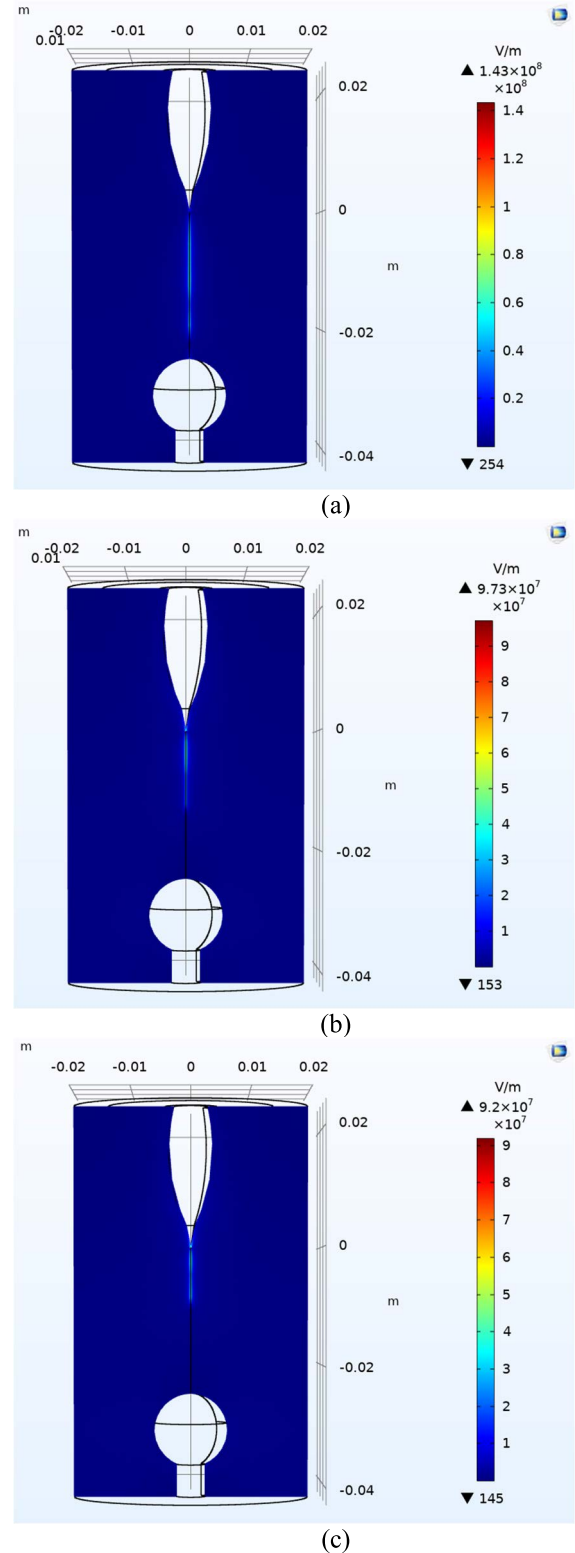


**FIGURE 15.** Electric field distribution in 3D across the gap at  $t = 15 \mu s$  after the application of the 75 kV LIV for: (a) Matrix oil, (b) TNF, (c) sNF.

tively.

$$H(p_{np,sat} - p_{np}) = \begin{cases} 0, & |\rho_{np}| \leq |\rho_{np-sat}| \\ 1, & |\rho_{np}| > |\rho_{np-sat}| \end{cases} \quad (16)$$

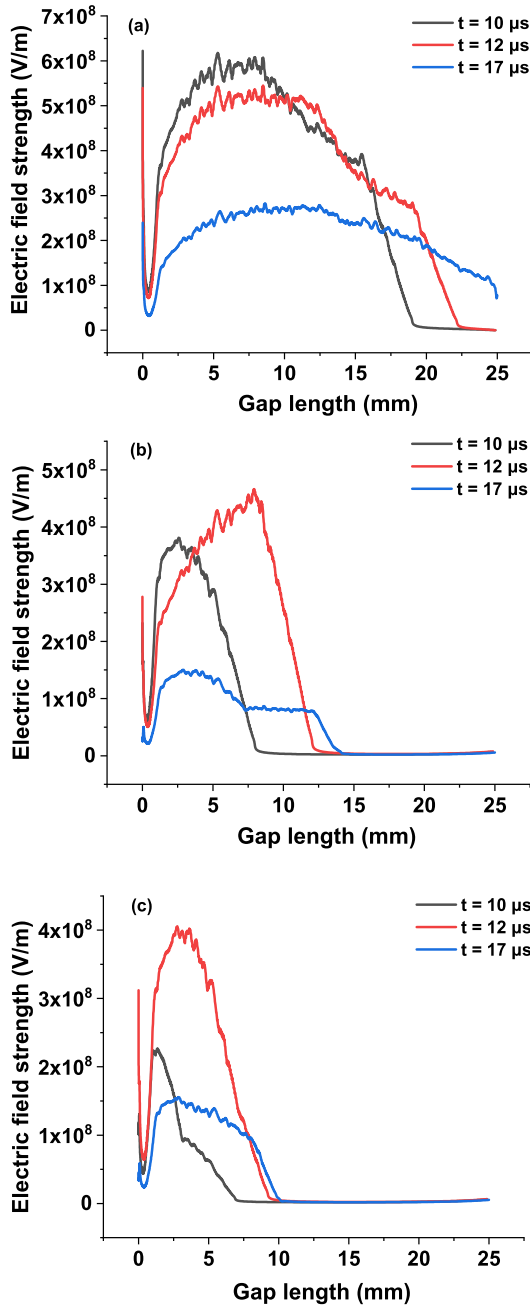


**FIGURE 16.** Electric field distribution across the gap at  $t = 10, 12$  and  $17 \mu s$  after the application of the 75 kV LIV for: (a) Matrix oil, (b) tNF, (c) sNF.

The ion-ion,  $R_{pn}$ , and ion-electron,  $R_{pe}$ , recombination rates have been calculated from (17) and (18) respectively [23]:

$$R_{pn} = \frac{e(\mu_+ + \mu_-)}{\varepsilon'_1} \quad (17)$$

$$R_{pe} = \frac{e(\mu_+ + \mu_e)}{\varepsilon'_1} \quad (18)$$

Lastly, the electric field ionization charge density rate  $G_I \left( \left| \vec{E} \right| \right)$  has been calculated based on Zener formula (19)

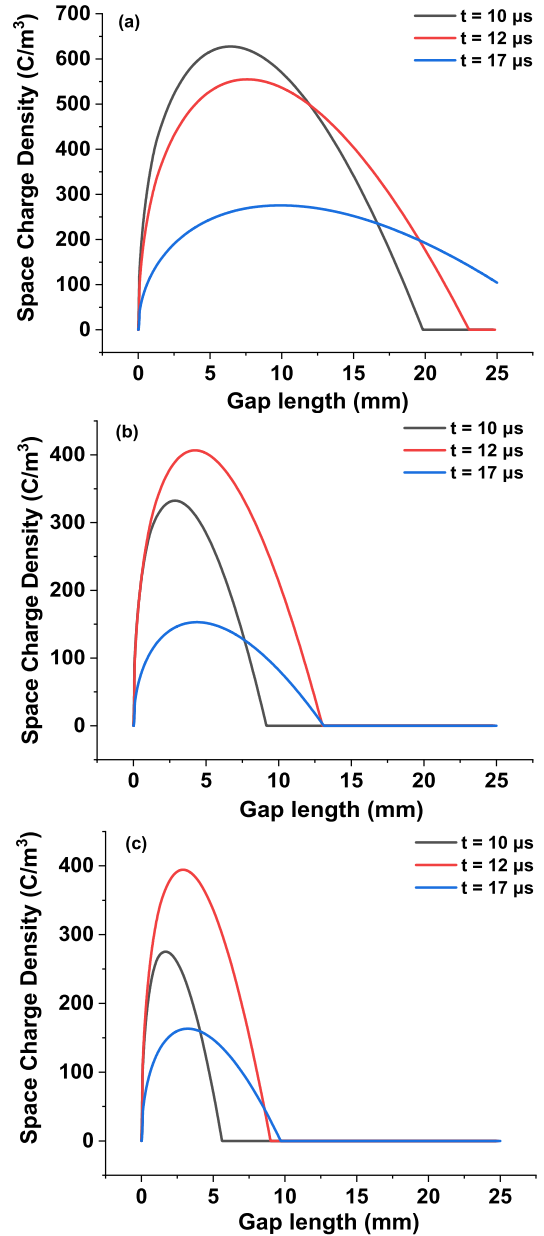


**FIGURE 17.** Space charge density across the gap at  $t = 10, 12$  and  $17 \mu s$  after the application of the 75 kV LIV for: (a) Matrix oil, (b) tNF, (c) sNF.

[23], [25]:

$$G_I \left( \left| \vec{E} \right| \right) = \frac{e^2 n_0 a \left| \vec{E} \right|}{h} \exp \left( - \frac{\pi^2 m^* \alpha \Delta^2}{eh^2 \left| \vec{E} \right|} \right) \quad (19)$$

where,  $\left| \vec{E} \right|$  is the electric field ionization threshold, determined to be  $1 \times 10^8$  V/m in this work.

The definition of the variables that appear in the aforementioned Equations is provided in Table 5, along with their values used for the simulation scenarios based on previous works [23], [25]. For every simulation case, a LI voltage (1.2/50  $\mu s$ ) is applied at the positive point electrode with peak

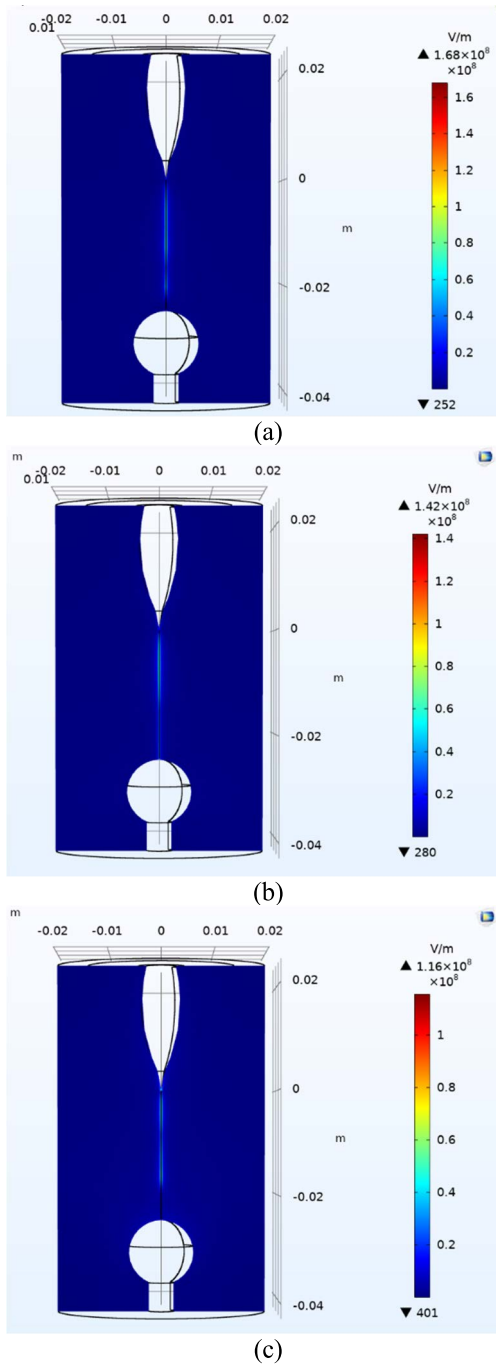


**FIGURE 18.** Electric field distribution in 3D across the gap at  $t = 15 \mu s$  after the application of the 80 kV LIV for: (a) Matrix oil, (b) tNF, (c) sNF.

values of 75 (Fig. 13 (a)) and 80 kV (Fig. 13 (b)) for the three under study oil samples. The gap with the point-sphere geometry according to IEC 60897 standard, imported in COMSOL Multiphysics, is depicted in Figure 14(a). The free triangular mesh distribution used to distinguish the geometry is presented in Figure 14(b). The duration of each simulation case was  $20 \mu s$  with a time step of  $0.5 \mu s$ . For every LIV voltage level, the electric field distribution and space charge density across the 2.5 cm gap have been recorded at selected

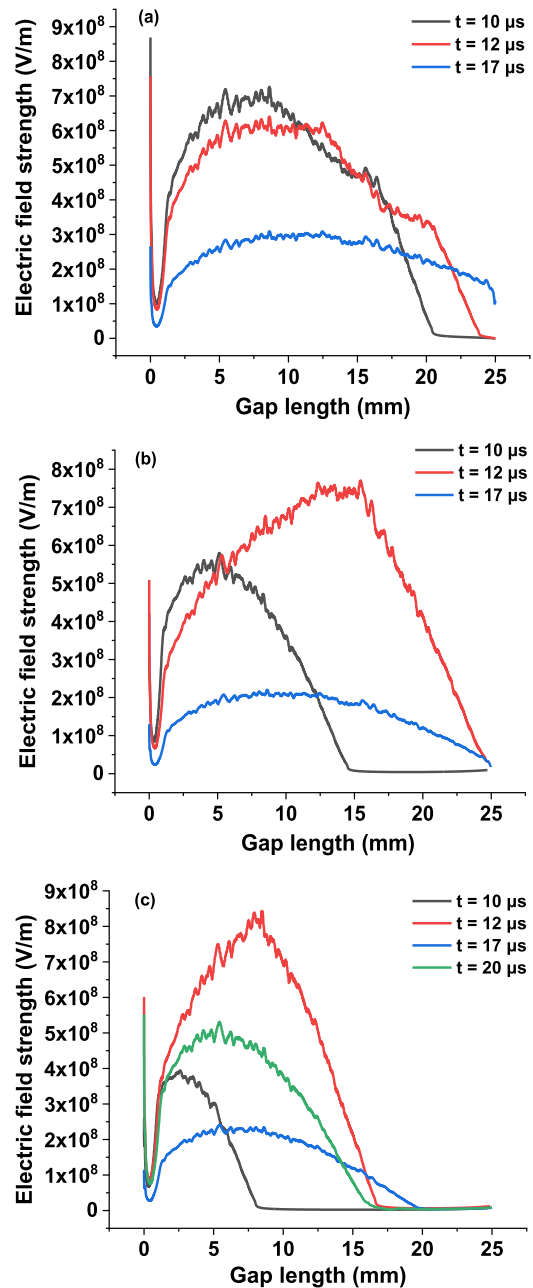


**FIGURE 19.** Electric field distribution across the gap at  $t = 10, 12$  and  $17 \mu s$  after the application of the 80 kV LIV for (a) Matrix oil, (b) tNF and  $t = 10, 12, 17$  and  $20 \mu s$  for (c) sNF.

time intervals, i.e. at  $10, 12$  and  $17 \mu s$  after the application of the LIV at the positive point electrode. Apart from that, the electric field strength across the gap at  $t = 15 \mu s$  has been illustrated in 3D for every under-study sample at each LIV level.

#### A. LIGHTNING IMPULSE VOLTAGE LEVEL OF 75 KV

Figure 15(a)-(c) depicts the electric field distribution across the gap  $15 \mu s$  after the application of the positive LIV in terms of the matrix, tNF and sNF samples respectively. From

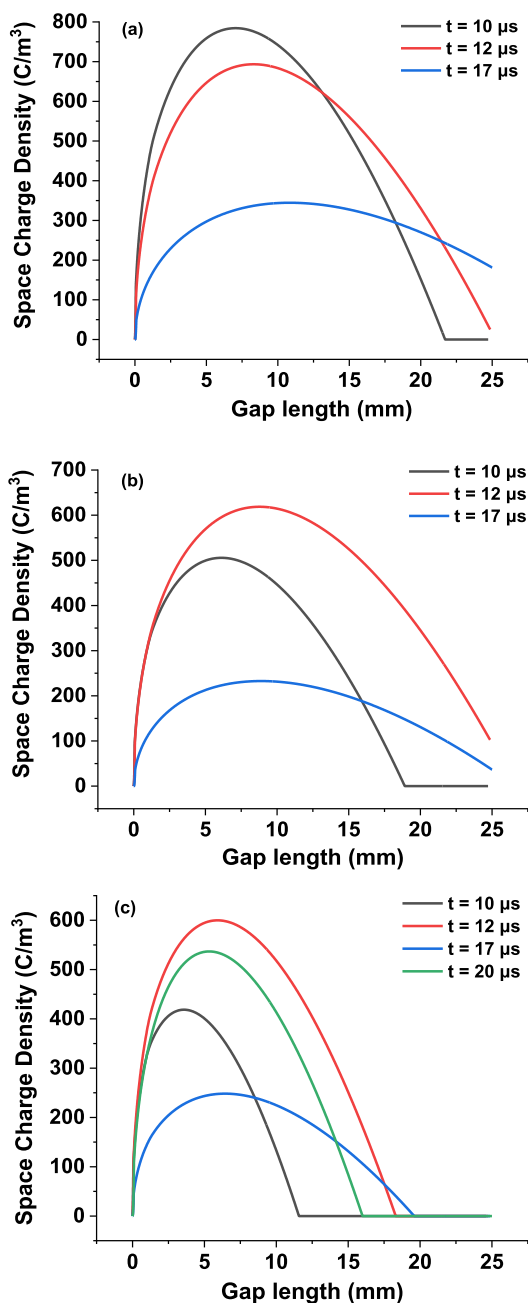


**FIGURE 20.** Space charge density across the gap at  $t = 10, 12$  and  $17 \mu\text{s}$  after the application of the 75 kV LIV for: (a) Matrix oil, (b) tNF, (c) sNF.

these plots, it is evident that, in the case of the matrix oil, the streamer has propagated significantly towards the negative sphere electrode and could cause breakdown, unlike the two NFs. This is clearer from the electric field and space charge plots of Figures 16(a)-(c) and 17(a)-(c) respectively. Higher electric field and space charge values across the gap are recorded for the matrix oil case, which extend across the whole gap. In fact, based on Figure 16(a) and 17(a) it seems that at  $t = 17 \mu\text{s}$  the gap is bridged, so the 75 kV LIV could be a possible candidate for BDV. In terms of the two NF samples, the electric field and space charge density are weakened and

restricted to 1.25 cm and 1 cm gap for the tNF and sNF respectively, with their values being more decreased for the sNF. It seems that the 75 kV LIV is not enough to cause breakdown in both NF samples due to the ability of NPs to act as electron scavengers, while the higher ability of SiC NPs is also demonstrated in simulation results through lower values of electric field and space charge density leading to delay of streamer propagation.

**B. LIGHTNING IMPULSE VOLTAGE LEVEL OF 80 kV**

Figure 18(a)-(c) depicts the electric field distribution across the gap 15 μs after the application of the positive LIV for the matrix oil, tNF and sNF samples respectively. Higher electric field values are recorded in relation to the first case, as expected, with matrix oil characterized from the highest, facilitating the breakdown, as observed from Figure 18(a). Figures 19(a)-(c) and 20(a)-(c) demonstrate the electric field and space charge density across the gap for the under-study samples. From Figures 19(b) and 20(b), which are referred to tNF, it seems that this voltage level is enough to cause the breakdown at about 17 μs after the LIV application. The space charge density across the gap significantly exceeds their saturation charge density, consequently the remaining charge is enough to bridge the gap and cause breakdown. Unlike the tNF sample, this voltage level does not cause breakdown of the sNF sample. As depicted in Figures 19(c) and 20(c), lower space charge density is accumulated in the gap hindering the streamer propagation, which however has bridged about 2 cm at 17 μs. For this reason, the depiction of electric field and space charge density distributions at 20 μs is necessary. Based on the same graphs, streamer propagation has receded to 1.5 cm, therefore it can be concluded that the breakdown with the application of 80 kV LIV has been avoided for the sNF sample. The results of the simulation at 75 and 80 kV LIV show a good match with the experimental ones presented in Section IV.

**VI. CONCLUSION**

In this work, a comparative study has been conducted regarding the influence of TiO<sub>2</sub> and SiC NPs at the same weight percentage ratio (0.004% w/w) on the thermal and dielectric performance of NEO FR3. The most important findings are summarized as follows:

- Both prepared NFs demonstrate great improvement of the thermal diffusivity and conductivity, with sNF’s conductivity mostly enhanced, by 58%, while the enhancement in terms of tNF is about 25%.
- The dielectric constant of both NF samples is decreased relatively to the matrix oil for a frequency range from 1-10<sup>6</sup> Hz, while all samples show decreased values of dielectric constant with temperature increase. sNF sample is characterized from the lowest dielectric constant, which is an indication that the addition of these kinds of NPs leads to a more insulating dielectric liquid.

- The DDF of both NF samples under room and high temperature is decreased with respect to NEO. However, DDF is increased for all of them with temperature rise.
- sNF sample shows the most improved LI BD strength under positive polarity, by around 10% with respect to the NEO.
- With the development of a numerical model, it has been shown that greater values of electric field and space charge density are recorded at LIV level of 75 kV for the Matrix oil, while the sNF sample demonstrates the lowest ones both at 75 and 80 kV levels, verifying the experimental results.

As part of future work, it would be of major interest to compare the numerical simulation results to the ones of NFs suffering from rapid aggregation, in order to verify the influence of NPs' agglomeration on the reduction of dielectric strength.

### ACKNOWLEDGMENT

The authors want to express their gratitude to Dr. Aspasia Antonelou from the Foundation for Research and Technology Hellas, Institute of Chemical Engineering Sciences, Patras, Greece for the FE-SEM images and the assistance in the synthesis of the NF samples; and Aimilia Barmdaki from the Condensed Matter Division, Department of Physics, University of Patras, for the assistance in the conduction of measurements of dielectric constant and electrical conductivity of the NPs. They would like to thank Mr. Konstantinos Giotis from the High Voltage Laboratory, Department of Electrical and Computer Engineering, University of Patras, for editing of the equivalent circuit of Figure 5a; and Alexis Chorozoglou for the Comsol post-processing. The computational resources for this study were kindly provided by the Environmental Research Laboratory of the National Center for Scientific Research Demokritos.

### REFERENCES

- [1] M. Rafiq, M. Shafique, A. Azam, and M. Ateeq, "Transformer oil-based nanofluid: The application of nanomaterials on thermal, electrical and physicochemical properties of liquid insulation—A review," *Ain Shams Eng. J.*, vol. 12, no. 1, pp. 555–576, Mar. 2021.
- [2] M. M. M. Salama, D.-E.-A. Mansour, M. Daghrah, S. M. Abdelkassoud, and A. A. Abbas, "Thermal performance of transformers filled with environmentally friendly oils under various loading conditions," *Int. J. Electr. Power Energy Syst.*, vol. 118, Jun. 2020, Art. no. 105743.
- [3] U. M. Rao, I. Fofana, A. Beroual, P. Rozga, M. Pompili, L. Calcara, and K. J. Rapp, "A review on pre-breakdown phenomena in ester fluids," *IEEE Trans. Dielectr. Electr. Insul.*, vol. 27, no. 5, pp. 1546–1560, Oct. 2020.
- [4] M. Pompili, C. Mazzetti, and R. Bartnikas, "Early stages of negative PD development in dielectric liquids," *IEEE Trans. Dielectr. Electr. Insul.*, vol. 2, no. 4, pp. 602–613, Aug. 1995.
- [5] U. M. Rao, I. Fofana, T. Jaya, E. M. Rodriguez-Celis, J. Jalbert, and P. Picher, "Alternative dielectric fluids for transformer insulation system: Progress, challenges, and future prospects," *IEEE Access*, vol. 7, pp. 184552–184571, 2019.
- [6] M. Daghrah, Z. Wang, Q. Liu, A. Hilker, and A. Gyore, "Experimental study of the influence of different liquids on the transformer cooling performance," *IEEE Trans. Power Del.*, vol. 34, no. 2, pp. 588–595, Apr. 2019.
- [7] P. Thomas, N. E. Hudedmani, R. T. A. R. Prasath, N. K. Roy, and S. N. Mahato, "Synthetic ester oil based high permittivity CaCu<sub>3</sub>Ti<sub>4</sub>O<sub>12</sub> (CCTO) nanofluids an alternative insulating medium for power transformer," *IEEE Trans. Dielectr. Electr. Insul.*, vol. 26, no. 1, pp. 314–321, Jan. 2019.
- [8] Y. Zhong, Y. Lv, C. Li, Y. Du, M. Chen, S. Zhang, Y. Zhou, and L. Chen, "Insulating properties and charge characteristics of natural ester fluid modified by TiO<sub>2</sub> semiconductive nanoparticles," *IEEE Trans. Dielectr. Electr. Insul.*, vol. 20, no. 1, pp. 135–140, Feb. 2013.
- [9] M. R. Hussain, Q. Khan, A. A. Khan, S. S. Refaat, and H. Abu-Rub, "Dielectric performance of magneto-nanofluids for advancing oil-immersed power transformer," *IEEE Access*, vol. 8, pp. 163316–163328, 2020.
- [10] G. D. Peppas, V. P. Charalampakos, E. C. Pyrgioti, M. G. Danikas, A. Bakandritsos, and I. F. Gonos, "Statistical investigation of AC breakdown voltage of nanofluids compared with mineral and natural ester oil," *IET Sci. Meas. Technol.*, vol. 10, no. 6, pp. 644–652, Sep. 2016.
- [11] M. Beroual and U. Khaled, "Statistical investigation of lightning impulse breakdown voltage of natural and synthetic ester oils-based Fe<sub>3</sub>O<sub>4</sub>, Al<sub>2</sub>O<sub>3</sub> and SiO<sub>2</sub> nanofluids," *IEEE Access*, vol. 8, pp. 112615–112623, 2020.
- [12] M. Jaroszewski, A. Beroual, and D. Golebiowski, "Effect of temperature on dielectric loss factor of biodegradable transformer oil," in *Proc. IEEE Int. Conf. High Voltage Eng. Appl. (ICHVE)*, Athens, Greece, Sep. 2018, pp. 1–4.
- [13] K. N. Koutras, S. N. Tegopoulos, V. P. Charalampakos, A. Kyritsis, I. F. Gonos, and E. C. Pyrgioti, "Breakdown performance and partial discharge development in transformer oil-based metal carbide nanofluids," *Nanomaterials*, vol. 12, no. 2, p. 269, Jan. 2022.
- [14] Z. B. Siddique, S. Basu, and P. Basak, "Dielectric behavior of natural ester based mineral oil blend dispersed with TiO<sub>2</sub> and ZnO nanoparticles as insulating fluid for transformers," *J. Mol. Liquids*, vol. 339, Oct. 2021, Art. no. 116825.
- [15] U. Khaled and A. Beroual, "AC dielectric strength of synthetic ester-based Fe<sub>3</sub>O<sub>4</sub>, Al<sub>2</sub>O<sub>3</sub> and SiO<sub>2</sub> nanofluids—Conformity with normal and Weibull distributions," *IEEE Trans. Dielectr. Electr. Insul.*, vol. 26, no. 2, pp. 625–633, Mar. 2019.
- [16] J. Jacob, P. Preetha, and T. K. Sindhu, "Stability analysis and characterization of natural ester nanofluids for transformers," *IEEE Trans. Dielectr. Electr. Insul.*, vol. 27, no. 5, pp. 1715–1723, Oct. 2020.
- [17] K. N. Koutras, I. A. Naxakis, A. E. Antonelou, V. P. Charalampakos, E. C. Pyrgioti, and S. N. Yannopoulos, "Dielectric strength and stability of natural ester oil based TiO<sub>2</sub> nanofluids," *J. Mol. Liquids*, vol. 316, Oct. 2020, Art. no. 113901.
- [18] H. Khelifa, E. Vagnon, and A. Beroual, "AC breakdown voltage and partial discharge activity in synthetic ester-based fullerene and graphene nanofluids," *IEEE Access*, vol. 10, pp. 5620–5634, 2022.
- [19] R. A. Farade, N. I. A. Wahab, D.-E.-A. Mansour, N. B. Azis, J. B. Jasni, V. Veerasamy, M. Thirumeni, A. X. R. Irudayaraj, and A. S. Murthy, "Investigation of the effect of sonication time on dispersion stability, dielectric properties, and heat transfer of graphene based green nanofluids," *IEEE Access*, vol. 9, pp. 50607–50623, 2021.
- [20] D. D. H. Fontes, G. Ribatski, and E. P. B. Filho, "Experimental evaluation of thermal conductivity, viscosity and breakdown voltage AC of nanofluids of carbon nanotubes and diamond in transformer oil," *Diamond Rel. Mater.*, vol. 58, pp. 115–121, Sep. 2015.
- [21] B. X. Du and X. L. Li, "High thermal conductivity transformer oil filled with BN nanoparticles," *IEEE Trans. Dielectr. Electr. Insul.*, vol. 22, no. 2, pp. 851–858, Apr. 2015.
- [22] R. A. Farade, N. I. B. A. Wahab, D.-E.-A. Mansour, N. B. Azis, J. Jasni, N. R. Banapurmath, and M. E. M. Soudagar, "Investigation of the dielectric and thermal properties of non-edible cottonseed oil by infusing h-BN nanoparticles," *IEEE Access*, vol. 8, pp. 76204–76217, 2020.
- [23] J. G. Hwang, M. Zahn, F. M. O'Sullivan, L. A. A. Pettersson, O. Hjortstam, and R. Liu, "Effects of nanoparticle charging on streamer development in transformer oil-based nanofluids," *J. Appl. Phys.*, vol. 107, no. 1, Jan. 2010, Art. no. 014310.
- [24] E. G. Atiya, D.-E.-A. Mansour, R. M. Khattab, and A. M. Azmy, "Dispersion behavior and breakdown strength of transformer oil filled with TiO<sub>2</sub> nanoparticles," *IEEE Trans. Dielectr. Electr. Insul.*, vol. 22, no. 5, pp. 2463–2472, Oct. 2015.
- [25] W. Sima, J. Shi, Q. Yang, S. Huang, and X. Cao, "Effects of conductivity and permittivity of nanoparticle on transformer oil insulation performance: Experiment and theory," *IEEE Trans. Dielectr. Electr. Insul.*, vol. 22, no. 1, pp. 380–390, Feb. 2015.

- [26] H. Duzkaya and A. Beroual, "Statistical analysis of AC dielectric strength of natural ester-based ZnO nanofluids," *Energies*, vol. 14, no. 1, p. 99, Dec. 2020.
- [27] V. A. Primo, B. García, J. C. Burgos, and D. Pérez-Rosa, "Investigation of the lightning impulse breakdown voltage of mineral oil based Fe<sub>3</sub>O<sub>4</sub> nanofluids," *Coatings*, vol. 9, no. 12, p. 799, Nov. 2019.
- [28] D.-E.-A. Mansour, A. M. Elsaed, and M. A. Izzularab, "The role of interfacial zone in dielectric properties of transformer oil-based nanofluids," *IEEE Trans. Dielectr. Electr. Insul.*, vol. 23, no. 6, pp. 3364–3372, Dec. 2016.
- [29] M. M. Bhunia, K. Panigrahi, C. B. Naskar, S. Bhattacharjee, K. K. Chattopadhyay, and P. Chattopadhyay, "2D square nanosheets of anatase TiO<sub>2</sub>: A surfactant free nanofiller for transformer oil nanofluids," *J. Mol. Liquids*, vol. 325, Mar. 2021, Art. no. 115000.
- [30] J. Chen, P. Sun, W. Sima, Q. Shao, L. Ye, and C. Li, "A promising nano-insulating-oil for industrial application: Electrical properties and modification mechanism," *Nanomaterials*, vol. 9, no. 5, p. 788, May 2019.
- [31] E. G. Atiya, D.-E.-A. Mansour, and M. A. Izzularab, "Partial discharge development in oil-based nanofluids: Inception, propagation and time transition," *IEEE Access*, vol. 8, pp. 181028–181035, 2020.
- [32] N. M. K. Abdel-Gawad, D.-E.-A. Mansour, A. Z. El Dein, H. M. Ahmed, and M. M. F. Darwish, "Effect of functionalized TiO<sub>2</sub> nanoparticles on dielectric properties of PVC nanocomposites used in electrical insulating cables," in *Proc. 18th Int. Middle East Power Syst. Conf. (MEPCON)*, Dec. 2016, pp. 693–698.
- [33] N. M. K. Abdel-Gawad, A. Z. El Dein, D. A. Mansour, H. M. Ahmed, M. M. F. Darwish, and M. Lehtonen, "Development of industrial scale PVC nanocomposites with comprehensive enhancement in dielectric properties," *IET Sci., Meas. Technol.*, vol. 13, no. 1, pp. 90–96, Jan. 2019.
- [34] D.-E.-A. Mansour, N. M. K. Abdel-Gawad, A. Z. El Dein, H. M. Ahmed, M. M. F. Darwish, and M. Lehtonen, "Recent advances in polymer nanocomposites based on polyethylene and polyvinylchloride for power cables," *Materials*, vol. 14, no. 1, p. 66, Dec. 2020.
- [35] V. S. Chaudhary, D. Kumar, G. P. Mishra, S. Sharma, and S. Kumar, "Plasmonic biosensor with gold and titanium dioxide immobilized on photonic crystal fiber for blood composition detection," *IEEE Sensors J.*, vol. 22, no. 9, pp. 8474–8481, May 2022.
- [36] V. S. Chaudhary, D. Kumar, and S. Kumar, "Gold-immobilized photonic crystal fiber-based SPR biosensor for detection of malaria disease in human body," *IEEE Sensors J.*, vol. 21, no. 16, pp. 17800–17807, Aug. 2021.
- [37] V. S. Chaudhary, D. Kumar, and S. Kumar, "SPR-assisted photonic crystal fiber-based dual-wavelength single polarizing filter with improved performance," *IEEE Trans. Plasma Sci.*, vol. 49, no. 12, pp. 3803–3810, Dec. 2021.
- [38] N. A. Azizie and N. Hussin, "Preparation of vegetable oil-based nanofluid and studies on its insulating property: A review," *J. Phys. Conf.*, vol. 1432, Jan. 2020, Art. no. 012025.
- [39] A. Hameed, A. Mukhtar, U. Shafiq, M. Qizilbash, M. S. Khan, T. Rashid, C. B. Bavoh, W. U. Rehman, and A. Guardo, "Experimental investigation on synthesis, characterization, stability, thermo-physical properties and rheological behavior of MWCNTs-kapok seed oil based nanofluid," *J. Mol. Liquids*, vol. 277, pp. 812–824, Mar. 2019.
- [40] A. Naddaf and S. Z. Heris, "Experimental study on thermal conductivity and electrical conductivity of diesel oil-based nanofluids of graphene nanoplatelets and carbon nanotubes," *Int. Commun. Heat Mass Transf.*, vol. 95, pp. 116–122, Jul. 2018.
- [41] G. Chen, J. Li, F. Wang, Z. Huang, L. Dan, and Y. Duan, "Branching initial streamers to inhibit the streamer propagation in natural ester-based nanofluid," *IEEE Trans. Dielectr. Electr. Insul.*, vol. 28, no. 1, pp. 116–123, Feb. 2021.
- [42] M. M. Emara, G. D. Peppas, A. D. Polykrati, S. Tegopoulos, E. C. Pyrgioti, D. D. Chronopoulos, A. Kyritsis, and I. F. Gonos, "Thermal and electrical conductivities for ester oil based graphene nana-sheets," in *Proc. IEEE Int. Conf. High Voltage Eng. Appl. (ICHVE)*, Beijing, China, Sep. 2020, pp. 1–4.
- [43] *Standard Test Method for Water Using Volumetric Karl Fischer Titration*, Standard ASTM D1533-00(2005), 2005.
- [44] N. M. K. Abdel-Gawad, A. Z. El Dein, D. A. Mansour, H. M. Ahmed, M. M. F. Darwish, and M. Lehtonen, "PVC nanocomposites for cable insulation with enhanced dielectric properties, partial discharge resistance and mechanical performance," *High Voltage*, vol. 5, no. 4, pp. 463–471, Aug. 2020.
- [45] P. A. Klonos, S. N. Tegopoulos, C. S. Koutsira, E. Kontou, P. Pissis, and A. Kyritsis, "Effects of CNTs on thermal transitions, thermal diffusivity and electrical conductivity in nanocomposites: Comparison between an amorphous and a semicrystalline polymer matrix," *Soft Matter*, vol. 15, no. 8, pp. 1813–1824, 2019.
- [46] E. Marx, *Hochspannungs-Praktikum*. Berlin, Germany: Springer, 1952.
- [47] *Methods for the Determination of the Lightning Impulse Breakdown Voltage of Insulating Liquids*, Standard IEC 60897, 1987.
- [48] D. Li, Z. Zhang, S. Liu, and S. Li, "An improved polarization model to analyze the breakdown strength of nano-liquid under impulse breakdown test," *IET Micro Nano Lett.*, vol. 16, no. 9, pp. 448–454, Aug. 2021.
- [49] H. J. Wang, S. J. Ma, H. M. Yu, Q. Zhang, C. M. Guo, and P. Wang, "Thermal conductivity of transformer oil from 253 K to 363 K," *Petroleum Sci. Technol.*, vol. 32, no. 17, pp. 2143–2150, 2014.
- [50] M. M. Emara, G. D. Peppas, E. C. Pyrgioti, D. D. Chronopoulos, A. Bakandritsos, S. N. Tegopoulos, A. Kyritsis, T. E. Tsovilis, A. D. Polykrati, and I. F. Gonos, "Thermal and dielectric performance of ester oil based pentyl-graphene nanofluids," *IEEE Trans. Dielectr. Electr. Insul.*, vol. 29, no. 2, pp. 510–518, Apr. 2022.
- [51] X. Li, C. Zou, L. Zhou, and A. Qi, "Experimental study on the thermo-physical properties of diathermic oil based SiC nanofluids for high temperature applications," *Int. J. Heat Mass Transf.*, vol. 97, pp. 631–637, Jun. 2016.
- [52] Q. Luo, C. Wang, H. Wen, and L. Liu, "Research and optimization of thermophysical properties of sic oil-based nanofluids for data center immersion cooling," *Int. Commun. Heat Mass Transf.*, vol. 131, Feb. 2022, Art. no. 105863.
- [53] K. N. Koutras, A. E. Antonelou, I. A. Naxakis, V. P. Charalampakos, E. C. Pyrgioti, and S. N. Yannopoulos, "In-situ high temperature study of the long-term stability and dielectric properties of nanofluids based on TiO<sub>2</sub> and SiC dispersions in natural ester oil at various concentrations," *J. Mol. Liquids*, vol. 359, Aug. 2022, Art. no. 119284.
- [54] N. G. Trinh, C. Vincent, and J. Regis, "Statistical dielectric degradation of large-volume oil-insulation," *IEEE Power Eng. Rev.*, vols. PER-2, no. 10, pp. 30–31, Oct. 1982.
- [55] F. A. Rizk, *High Voltage Engineering*, 1st ed. Boca Raton, FL, USA: CRC Press, 2014, pp. 587–600.
- [56] M. Becerra, M. Aljure, A. M. Pourrahimi, and F. Roman, "High field conduction in mineral oil based ZnO nanofluids prior to negative streamer inception," *J. Phys. Commun.*, vol. 5, no. 4, Apr. 2021, Art. no. 045006.
- [57] *Insulation Co-Ordination—Part 1: Definitions, Principles and Rules*, Standard IEC 60071-1, 2019.
- [58] *Insulation Co-Ordination—Part 2: Application Guidelines*, Standard IEC 60071-2, 2018.
- [59] O. Lesaint and G. Massala, "Positive streamer propagation in large oil gaps: Experimental characterization of propagation modes," *IEEE Trans. Dielectr. Electr. Insul.*, vol. 5, no. 3, pp. 360–370, Jun. 1998.
- [60] Q. Liu and Z. Wang, "Streamer characteristic and breakdown in synthetic and natural ester transformer liquids under standard lightning impulse voltage," *IEEE Trans. Dielectr. Electr. Insul.*, vol. 18, no. 1, pp. 285–294, Feb. 2011.
- [61] *Protection Against Lightning—Part 4: Electrical and Electronic Systems Within Structures*, Standard IEC 62305-4, 2006.
- [62] J. Velasco, R. Frascella, R. Albarracín, J. Burgos, M. Dong, M. Ren, and L. Yang, "Comparison of positive streamers in liquid dielectrics with and without nanoparticles simulated with finite-element software," *Energies*, vol. 11, no. 2, p. 361, Feb. 2018.
- [63] J. Jadidian, "Charge transport and breakdown physics in liquid/solid insulation systems," Ph.D. thesis, Dept. Elect. Eng. Comput. Sci., MIT, Cambridge, MA, USA, 2013.



**KONSTANTINOS N. KOUTRAS** was born in Korinthos, Greece, in 1992. He received the Integrated master's degree in electrical and computer engineering and the M.Sc. degree in green electric power from the Department of Electrical and Computer Engineering, University of Patras, Greece, in 2016 and 2018, respectively, where he is currently pursuing the Ph.D. degree. He has authored/coauthored more than ten research papers published in journals and international conferences. His research interests include pre breakdown phenomena in dielectric liquids and preparation and study of nanofluids as an alternative insulative medium in power transformers and lightning protection.



**GEORGIOS D. PEPPAS** (Senior Member, IEEE) was born in Rustenburg, South Africa, in 1987. He received the Diploma degree in electrical engineering and the Ph.D. degree from the Department of Electrical and Computer Engineering, University of Patras, in 2011 and 2016, respectively. He has been a Research and Development Manager of Raycap leading innovation in surge protective devices and a Technical Manager of the High Current Laboratory of Raycap, since 2016. He is the author of four patents and of more than 39 papers in major scientific journals and conference proceedings. His research interests include lightning and surge protection and nanofluids for high-voltage applications.



**TIMOTHEOS T. FETSIS** was born in Agrinion, Greece, in 1998. He received the Integrated master's degree in electrical and computer engineering from the Department of Electrical and Computer Engineering, University of Patras, Greece, in 2022. His research interests include ionization channels, high-voltage simulations, and dielectric liquids.



**SOKRATIS N. TEGOPOULOS** was born in Athens, Greece, in 1977. He received the B.Sc. degree in natural sciences from Hellenic Open University, Patra, Greece, in 2016, and the M.Sc. degree in applied physics from the School of Applied Mathematical and Physical Sciences, National Technical University of Athens (NTUA), in 2018, where he is currently pursuing the Ph.D. degree. Within the research activity of the Dielectrics Group, he participates in research projects and assists in teaching undergraduate and postgraduate students. His main research interests include the study of structure-properties relationship in (bio)-polymer nanocomposite materials and hydration properties of several materials.



**VASSILIOS P. CHARALAMPAKOS** was born in Sparta, Greece, in 1975. He received the Diploma degree in electrical engineering and the Ph.D. degree from the Electrical and Computer Engineering Department, University of Patras, Greece, in 1998 and 2005, respectively. He is an Assistant Professor with the Electrical and Computer Engineering Department, University of Peloponnese. He has authored and coauthored more than 40 research papers in scientific journals and conference proceedings. His research interests include high-voltage systems, lightning protection, high-voltage insulation, dielectric liquids, and gaseous dielectrics.



**APOSTOLOS KYRITSIS** was born in Berlin, Germany in 1966. He received the Diploma degree in physics and the Ph.D. degree in materials science-physics from the University of Athens, Greece, in 1988 and 1995, respectively. He has published more than 165 scientific articles in major international peer-reviewed scientific journals and five book chapters. He has more than 210 contributions to international conferences and more than 50 to national conferences. His research interests include dielectric, thermal and vapor sorption studies in ionic crystals, ceramics, polymers and complex polymeric systems and structure-property relationships in polymers, biopolymers, nanocomposites, and hydration properties of inorganic and organic materials. He has been involved in national and international standardization activities and is strongly interested in the metrology aspects of experimental measurements.



**ANDREAS G. YIOTIS** was born in Athens, Greece, in 1974. He received the Diploma degree in chemical engineering and the Ph.D. degree in transport phenomena in porous media from the School of Chemical Engineering, National Technical University of Athens (NTUA), in 1997 and 2003, respectively. He is an Assistant Professor in fluid mechanics and petroleum engineering with the School of Mineral Resources Engineering, Technical University of Crete. He has published more than 35 articles in high quality peer-reviewed journals in the fields of multi-phase flows and hydrodynamic dispersion in porous, microfluidics, computational fluid mechanics, and hydrogen storage technologies.



**IOANNIS F. GONOS** (Senior Member, IEEE) was born in Artemisio, Arcadia, Greece, in 1970. He received the Diploma degree in electrical engineering and the Ph.D. degree from the National Technical University of Athens (NTUA), in 1993 and 2002, respectively. He is an Associate Professor with NTUA. He is the author of more than 200 papers in scientific journals and conferences proceedings. His research interests include grounding systems, dielectric liquids, high-voltages, measurements, and insulators.



**ELEFThERIA C. PYRGIOTI** (Member, IEEE) was born in Kanalia, Karditsa, Greece, in 1958. She received the Diploma degree in electrical engineering and the Ph.D. degree from the Electrical and Computer Engineering Department, University of Patras, Greece, in 1981 and 1991, respectively. She is Professor with the Electrical and Computer Engineering Department, University of Patras. Her research interests include high-voltage systems, lightning protection, high-voltage insulation, dielectric liquids distributed generation, and renewable energy.

...